

A new sampling methodology for creating rich, heterogeneous, subsets of samples for training image segmentation algorithms

Matheus Viana da Silva,¹ Natália de Carvalho Santos,² Baptiste Lacoste,³ and Cesar H. Comin^{1,*}

¹*Department of Computer Science, Federal University of São Carlos, São Carlos, SP, Brazil*

²*São Carlos Institute of Physics, University of São Paulo, Av. Trab. São Carlense,
400. Parque Arnold Schmidt, São Carlos, SP, 13566-590, Brazil*

³*Department of Cellular and Molecular Medicine, Faculty of Medicine, University of Ottawa, Ottawa, ON, Canada*

(Dated: January, 2023)

Creating a dataset for training supervised machine learning algorithms can be a demanding task. This is especially true for medical image segmentation since this task usually requires one or more specialists for image annotation, and creating ground truth labels for just a single image can take up to several hours. In addition, it is paramount that the annotated samples represent well the different conditions that might affect the imaged tissue as well as possible changes in the image acquisition process. This can only be achieved by considering samples that are typical in the dataset as well as atypical, or even outlier, samples. We introduce a new sampling methodology for selecting relevant images from a larger non-annotated dataset in a way that evenly considers both prototypical as well as atypical samples. The methodology involves the generation of a uniform grid from a feature space representing the samples, which is then used for randomly drawing relevant images. The selected images provide a uniform cover of the original dataset, and thus define a heterogeneous set of images that can be annotated and used for training supervised segmentation algorithms. We provide a case example by creating a dataset containing a representative set of blood vessel microscopy images selected from a larger dataset containing thousands of images.

I. INTRODUCTION

Recent developments in neural networks led to unprecedented results in image classification [1, 2], object detection [3] and image segmentation [4]. Neural networks, and the related field of Deep Learning, shifted the prevalent focus on feature engineering to a more data-centric approach, where network models can approximate highly complex functions provided the model has enough capacity and the dataset is sufficiently representative [5]. Due to such impressive advancements, many authors argue that neural networks have reached human-level accuracy in some tasks [6–10].

The performance of neural networks has dominantly been measured using metrics such as classification or segmentation accuracy, precision, recall, and the area under the ROI curve. However, recent studies have shown the dangers of only considering such globally-averaged metrics [11–13] that provide only an aggregated, summarized, view of the performance of machine learning algorithms on datasets with sometimes millions of images. Such an approach may hide important biases of the model [13]. For instance, for medical images, a 95% accuracy is usually considered a good performance. But what about the remaining 5%? It is unrealistic to expect models to reach 100% accuracy, but the samples that are not correctly processed by a neural network may hide important biases of the model. These concerns led to the definition of new approaches and metrics that can aid the interpretation of black box models [14].

For the task of segmentation in medical images, which is the focus, but not the only application of our study, the detection of the important structures is usually only the first step of a more elaborate procedure for measuring relevant properties such as size [15], regularity [16], length [17, 18], and curvature [18, 19]. Therefore, systematic segmentation mistakes might lead to undetected errors when characterizing samples for clinical diagnoses [20] and research purposes [11]. An important cause of such systematic errors can be the presence of samples having characteristics that occur with low frequency in a dataset. This can happen due to additional, unexpected, noise during image acquisition, variations in tissue staining, image artifacts, or even the presence of structures that are anatomically different than what was expected. Assuming for illustration purposes that the data is normally distributed, a machine learning model having good performance around the peak of the distribution will tend to have good average accuracy measured for the whole dataset, even if it cannot correctly classify or segment images that are around the tail of the distribution, which might be important for downstream analyses. Notice that this discussion does not necessarily only involves outlier images, but any image occurring with a low probability according to some criteria. Nevertheless, the concept of *outlier* has been given different definitions [21, 22], and it sometimes is used as a synonym for *low probability*.

Here we argue that a machine learning model should have good performance, or even be directly optimized, on both prototypical and atypical samples. This focus can lead to models that are more robust to samples located in a sparsely populated region of the feature space of the dataset. In addition, it might also lead to models that

* Corresponding author: chcomin@gmail.com

generalize better to out-of-distribution samples as well as to new datasets. We develop a simple and intuitive sampling methodology to select a subset of images from the dataset representing, as best as possible, a uniform coverage of the feature space of all the samples. This subset can be used for measuring the homogeneity of the performance of the model on highly distinct samples. It can also be used for identifying regions in the feature space where the model does not perform well.

We focus on applying the method to the important segmentation problem of selecting relevant samples for ground truth mask annotation. For medical images, manually annotating masks can be very time consuming and requires skilled workers or specialists. Therefore, when many samples are available for annotation, it is interesting to select an optimal subset of samples that leads to a model that is also expected to perform well on the whole dataset. To this end, we present a case example of selecting an appropriate subset of samples from a blood vessel dataset containing 2637 images. We show that the selected samples uniformly cover different properties of the images and thus represent a rich set of samples that can be annotated and used for training a segmentation algorithm for processing the whole dataset.

A concept that is similar to the developed methodology is the so-called *coreset* [23]. The aim of a coreset is to select a subset of samples that can optimally represent the whole dataset. Many different methodologies and criteria were developed for defining relevant coresets [23–25]. Indeed, the subset defined by our methodology can be associated with a coreset, but in our case, the aim of the generated subset and the approach used differs markedly from the usual definition of a coreset. The aim of our methodology is not focused on accurately representing the underlying distribution of the data, or on preserving the accuracy of a machine learning algorithm, but on providing a relevant dataset for training machine learning algorithms while avoiding the underrepresentation of atypical samples. In addition, many coreset methodologies use a surrogate neural network to estimate latent features or to estimate a degree of uncertainty about each sample, while our methodology is more general in the sense that any set of features obtained from the samples can be used. Those can even be specific features such as image contrast and average intensity. Furthermore, many studies consider a similarity metric for selecting relevant samples, which is a degenerate metric and therefore cannot provide a full representation of the data distribution. Our methodology also has some relationship with active learning [26–29]. But in our case, the whole subset of samples is generated in a single run and does not require an interactive session with a specialist.

II. METHODOLOGY

The sampling methodology proposed in this work can be divided into three steps: (a) dataset mapping to an n -

dimensional feature space, (b) generating a discrete representation of this feature space, and (c) drawing points uniformly from this feature space representation. We explain each of these steps in the following subsections.

A. Dataset mapping

Given a dataset $D = \{\delta_1, \delta_2, \dots, \delta_n\}$ with n objects, and a function $f : \delta_i \rightarrow \vec{p}_i$ that maps an object δ_i to a vector \vec{p}_i with dimension d , the new dataset mapped to a feature space can be represented as a $n \times d$ matrix. Each line of this matrix, which we call D_{mapped} , therefore represents the features of an object $f(\delta_i)$. Figure 1 illustrates this procedure for a set of images. Each image of the set (Figure 1(a)) is mapped to a point in the new feature space (Figure 1(b)).

There are many different approaches for defining $f(\delta_i)$. For example, if D is a set of images, we can map each image using a combination of relevant features, such as image contrast or signal-to-noise ratio. Feature mapping can also be achieved through a prior unsupervised or semi-supervised segmentation of the objects in the images. In this case, features such as object area or elongation can be used. Supervised learning can also be used to map the images to a new feature space. In this scenario, instead of mapping D through handcrafted features, the features learned by a supervised segmentation algorithm, such as a neural network, can be used. In Section III we present an example with a mapping function defined as a combination of global image features and handcrafted features from semi-supervised segmentation.

B. Feature space discretization

The second step of the sampling methodology is to define a regular grid in the feature space and to translate each data point to the nearest point in this grid. It is useful to first normalize the values of D_{mapped} to remove differences in the scale of the features. In this work, we used z-score normalization, but other normalizations can be used. After normalizing D_{mapped} , we proceed to *re-sample the mapped values to a discrete grid*. This is done by defining a scale ν that sets the size of each grid cell and calculating

$$D_{grid} = \text{floor} \left(\frac{D_{mapped}}{\nu} \right), \quad (1)$$

where *floor* is the floor function. As shown in Figure 1(c), this operation ensures that each value of D_{grid} lies within a regular grid. Note that, as a consequence of undersampling, we expect multiple data points to fall in the same grid position, this is one of the key properties of the method that will allow a uniform sampling of the data.

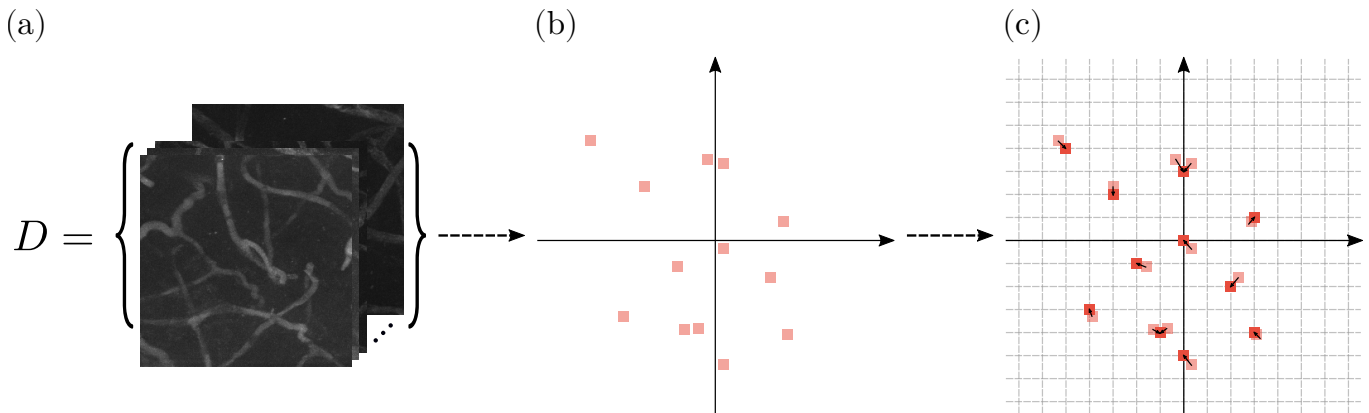


FIG. 1. Representation of the mapping procedure applied to a set D of samples, followed by the feature space discretization. Here, we consider D as a set of images. In this example, each image of D is mapped to a 2-d position in the new feature space (b). In (c), the mapped points (light-red points) are moved to a new position (red points) within a regular grid defined by Equation 1.

After feature space discretization, we generate a sparse set of points representing an estimation of the possible values that can be obtained in the feature space. We call this set the *sampling set* of the feature space. As illustrated in Figure 2, this procedure works as follows. An n -dimensional discrete hypersphere S with radius r (in grid units) centered on each data point is defined (Figure 2(a)). This hypersphere is translated to each data point position. The union of the calculated hypersphere positions of all points (Figure 2(b)) defines the sampling set D_{sset} .

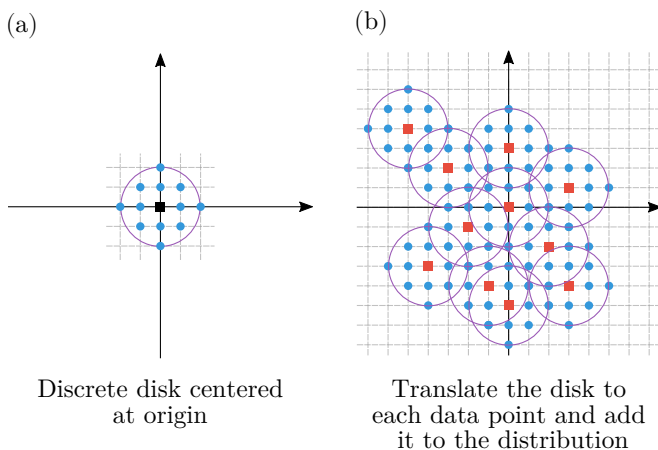


FIG. 2. Estimation of the feasible values of the feature space. In (a) we define a sparse hypersphere (depicted as a disk for visualization) as a set of uniformly distributed points. This disk is translated to the center of each point in D_{grid} (red points of (b)). The union of all hypersphere points defines D_{sset} .

Given that our algorithm operates over a discrete space, we expect repeated hypersphere points in D_{sset} after translation. These repeated values account for important information regarding the spatial distribution of the points in D_{sset} and can be stored and used to sample

the points in a non-uniform manner. Since the main goal of the presented methodology is to select heterogeneous subsets of the original data, which can optimally be done using a uniform distribution, we ignore repeated points in D_{sset} .

C. Uniform selection of samples

The last step of the sampling methodology consists of drawing a set of points from the sampling set D_{sset} . As illustrated in Figure 3, we draw from D_{sset} k points with uniform probability (green dots in Figure 3). For each point drawn, the closest data sample is identified using the Euclidean distance. If the same data sample is obtained more than once, a new point is drawn from D_{sset} until k unique data samples are obtained. The final set of data samples (orange stars in Figure 3) is represented as $D_{sampled}$.

As mentioned before, a uniform sampling of D_{sset} allows us to select prototypical and atypical samples of our dataset with equal probability. Nevertheless, one cannot guarantee that a random sampling of the estimated distribution will lead to a solution that maximizes the heterogeneity of the sampled subset. In particular, any given realization of the sampling may lead to distortions such as the selection of many samples at similar regions of the space or the creation of large regions with no samples selected. This is due to random fluctuations in the sampling. To amend this, we define a metric called Farthest Unselected Point (FUS), that punishes sampled subsets with large gaps between drawn points.

Being $D_{sampled}$ the set of sampled data points from D_{grid} , and $\neg D_{sampled}$ the set of points from D_{grid} that were not selected in the sampled subset, the FUS metric, as the name implies, measures the largest euclidean distance between any points of $\neg D_{sampled}$ and $D_{sampled}$. Sampled subsets leading to low values of the FUS metric

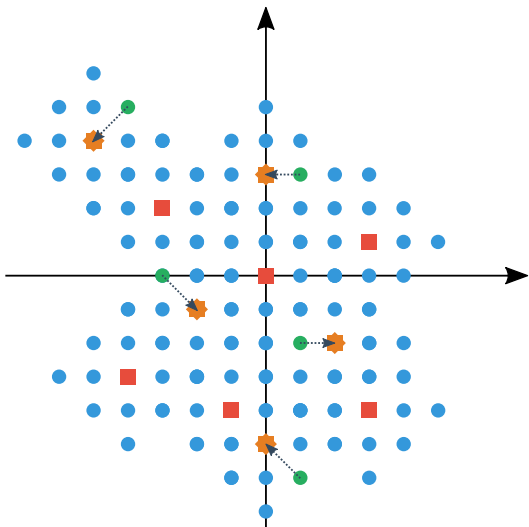


FIG. 3. Illustration of the proposed sampling protocol. k random points (green dots) are drawn from the sampling set D_{sset} (blue dots). The subset of sampled data points is defined by the data points that are closest to each drawn point (orange stars). Red squares represent the remaining data points that were not selected.

should be preferred, since it leads to lower gaps between points in $D_{sampled}$. This property is illustrated in Figure 4. In Figure 4(a), the farthest unselected point evidences a gap of sampled points in the upper right corner of the distribution. This gap is less pronounced in Figure 4(b), where the points are sampled more heterogeneously and unselected points are, in general, close to the sampled subset distribution. With that in mind, we ultimately choose $D_{sampled}$ as the set with the lowest FUS amongst N sampled subsets. In our experiments, we find that $N \geq 1000$ covers a good amount of subset possibilities, but the optimal value of N may change depending on the dataset being studied.

To illustrate the potential of the methodology, Figure 5 shows a comparison between the usual approach for selecting a subset of the data, to simply draw images at random with equal probability, and the selection of points using the presented method. Using uniform sampling, the points tend to be selected according to the underlying probability density function of the data, which is usually unknown. Thus, most of the selected points will tend to be located in denser regions of the feature space, which consequently biases the sampled subset towards the regions of the dataset with prototypical examples (Figure 5(a)). By drawing the subset of points using our methodology, the selected points will tend to cover the feature space more uniformly (Figure 5(b)).

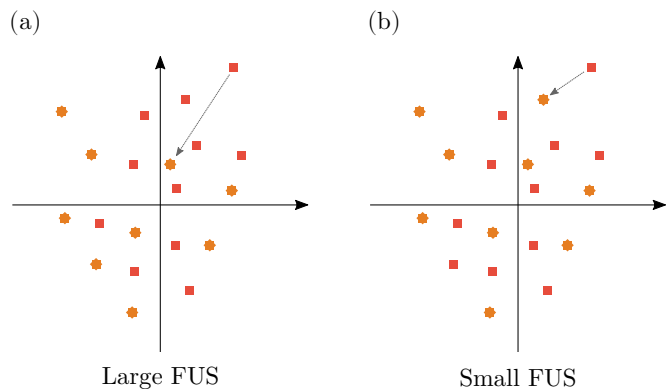


FIG. 4. An illustration of how minimizing the FUS metric also minimizes gaps between sampled points. In (a), a higher distance between unselected points (depicted as red squares) and sampled points (depicted as orange stars) indicates a large gap between sampled points. This behavior is less pronounced in (b), where a more heterogeneous subset was sampled.

III. CASE EXAMPLE – CREATING A DATASET FOR BLOOD VESSEL SEGMENTATION

To show the potential of the methodology, in this section we describe an application of the method on real data. We show how the method can aid in the selection of a heterogeneous set of samples that can then be used for training a supervised segmentation algorithm.

A. Blood vessel dataset

The dataset we will use contains confocal microscopy images of mouse brain vasculature. The dataset has 2637 images having sizes from 1376×1104 to 2499×2005 , totaling around 3.8GB of data. The images were acquired under different experimental conditions in different works published in the literature [30–32]. Conditions include control animals, animals that have suffered a deletion of chromosome 16p11.12, animals that have experienced sense deprivation or sense hyperarousal, samples from stroke regions, and also from different stages of mouse development.

This dataset is interesting because it has a considerable variety of characteristics of blood vessels. In addition, the images represent samples obtained from hundreds of different animals and experimental conditions. This makes it an excellent dataset for training machine learning algorithms for blood vessel segmentation. But training supervised algorithms requires the manual annotation of the blood vessels in a subset of the images.

After annotating a few samples, we estimated that each image in the dataset takes roughly 12 hours to fully annotate. Therefore, it is unfeasible to annotate the whole dataset. Thus, it is interesting to select relevant samples for annotation in order to train a machine learning algorithm to segment the whole dataset. As mentioned

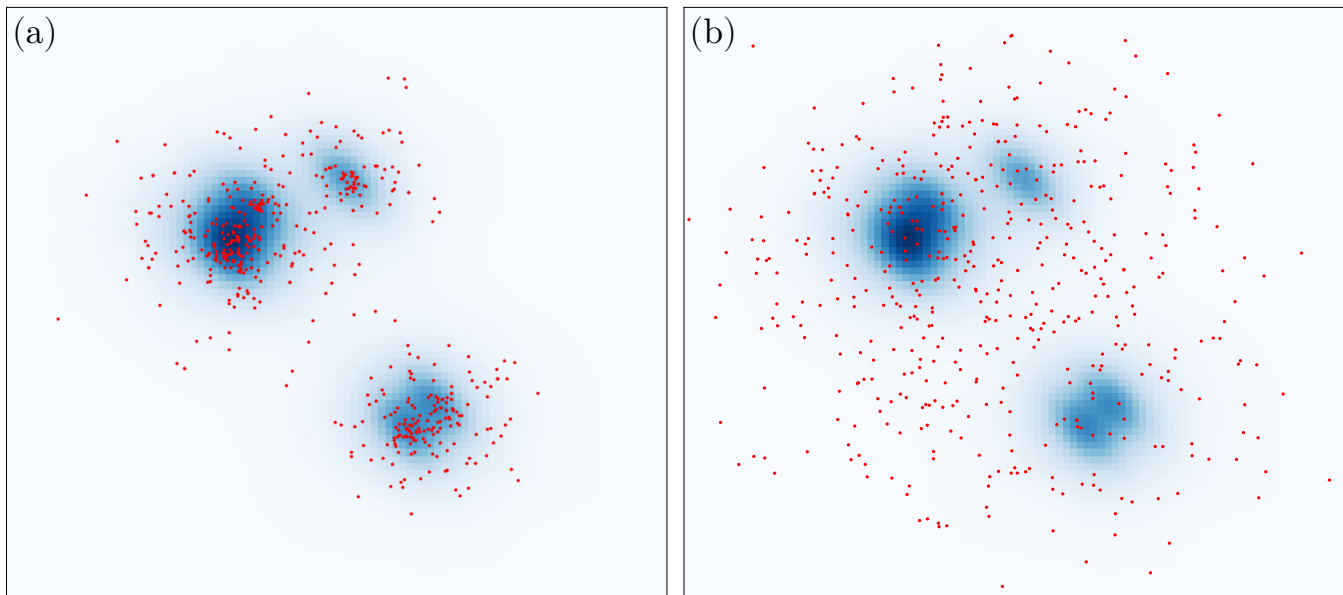


FIG. 5. Illustration of two sampling strategies. Red dots represent the sampled points. The background color represents the underlying probability density function of the data, with larger values having darker tones of blue. In (a), we have a typical example of uniformly sampling the indexes of a dataset, which leads to the selection of many samples that are similar to each other. In (b), the points are selected using the presented methodology. In this case, the sampled points are spread out and cover the feature space.

before, this subset of samples should allow the training to occur without biases, that is, atypical samples should be well-represented so that the accuracy of the algorithm depends as little as possible on the properties of the images or the tissues under analysis. This means that it is interesting to select both prototypical and atypical samples for annotation. The methodology presented in Section II was used for selecting the samples.

Each image in the dataset may include illumination inhomogeneities, changes in contrast, different levels of noise, as well as blood vessels having distinct characteristics (e.g., caliber, tortuosity, etc). Thus, from the original dataset, we generated a new set of images, each having a size of 256×256 . These smaller images were generated by extracting 256×256 regions from the original images. As shown in Figure 6, seven regions were extracted from each image. The seven regions were extracted in key areas of each image, with four windows in each of the corners of the image, a central window, and two windows at random positions. The latter two may overlap with the other windows. Windows that did not contain a satisfactory number of blood vessel segments were removed. The total size of the resulting dataset is 18279 images.

After obtaining the various extracted images, they were mapped to a feature space that was used for characterizing the samples. As mentioned in Section II A, image features can be calculated by processing labels obtained from semi-supervised segmentation. Since our dataset was used in previous works, each image has a respective segmentation that was obtained using a semi-supervised

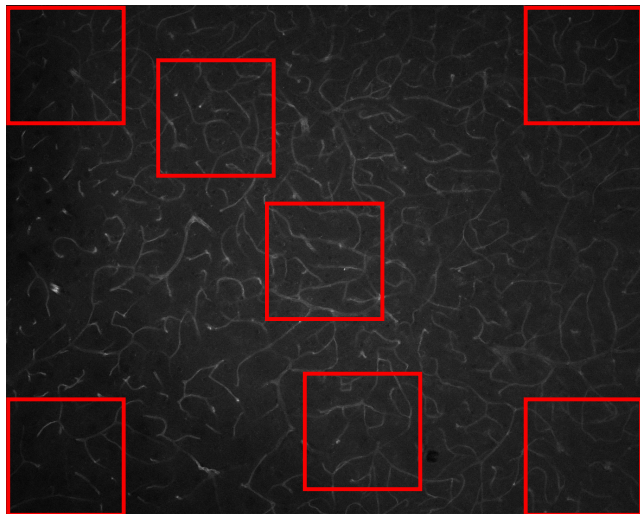


FIG. 6. An example of how we extract seven windows from a single sample. The four corners along with the central region can capture most of the illumination inhomogeneities that may occur due to uneven illumination of the samples. Besides these five regions, two additional random regions are also drawn for each image.

methodology. This methodology is based on the adaptive thresholding of the original images, where the threshold was selected manually for each image. The full details on the segmentation procedure are described in [18].

B. Metrics

We consider the following features to characterize the samples: blood vessel contrast, level of gaussian noise, blood vessel density, and medial line heterogeneity.

The blood vessel contrast is related to the difference in intensity between the vessels and the background of the image. The greater the contrast, the easier it is to detect the vessels. It can be measured using the original image of the vessels and the respective thresholded image containing an estimation of the pixels belonging to the vessels. The contrast is calculated as

$$C = \frac{\bar{I}_v}{\bar{I}_f}, \quad (2)$$

where \bar{I}_v and \bar{I}_f are the mean intensities of, respectively, the pixels belonging to the blood vessels and the background of the image.

The signal-to-noise level of the images can be estimated in different ways. We investigated different definitions and used the method that was the most compatible with a visual inspection of the images. The method proposed in [33] was used. It assumes a noise with normal distribution and uses wavelets to identify the most likely standard deviation of the noise component. To prevent the method from capturing vessel variation, only the background of the image was used for the estimation.

Blood vessel density is defined as the total length of blood vessels in an image divided by the image area. To do this, we first apply a skeletonization algorithm to extract the medial lines of the vessels. In this work, we used the Palágyi-Kuba algorithm [34]. The total length of vessels is calculated as the sum of the arc-lengths of all vessel segments. This metric is also fully explained in [18].

The last metric, which we call medial line heterogeneity, measures the illumination changes in the vessel lumen. To calculate this metric, we first blur the image using a gaussian filter with unit standard deviation to remove extreme values. The medial line heterogeneity is calculated as the standard deviation of the pixel values along the medial lines of this blurred image. The medial lines considered are the same ones used for the blood vessel density metric.

We observed that the medial line heterogeneity tends to be correlated with the average intensity of the blood vessels. In order to remove this dependency, the medial line heterogeneity as well as the average intensity of the medial lines was calculated for all images in the dataset. Then, a straight line fit $h_m = a * m + b$ was applied to the calculated values, where m is the average intensity and h_m is the expected medial line heterogeneity associated with m . Next, a normalized medial line heterogeneity was defined as $\tilde{h} = h - h_m$, where h is the medial line heterogeneity calculated for an image.

C. Subset sampling

With the four metrics described in the previous section, we mapped our dataset to a 4-d feature space by applying the methodology detailed in Section II A. As mentioned before, the dataset contains 18279 images. Hence, the whole dataset was mapped to a 18279×4 matrix. In the feature space discretization step (Section II B), we used z-score normalization and a scale of $\nu = 10$. The hypersphere was generated with a radius equal to four times the grid space resolution. In the sampling step (Section II C), we used $N = 1000$ and chose the sampling solution that minimized the FUS metric. The sampled subset size contained $k = 100$ images. To avoid data leaking, an additional restriction that prevented the selection of samples from the same image was used.

The generated subset contains a heterogeneous set of samples that can be used for annotation. It is difficult to properly measure the heterogeneity of this subset because it would involve the estimation of the probability density function of the original data, which is not a trivial task and can be influenced by the choice of parameter values. But it is clear that the method must naturally lead to a uniform selection of the samples. This is so because the set D_{grid} (defined in Section II B) represents an estimation of the domain of the probability density function of the data, and this domain is being sampled uniformly.

One approach to illustrate the characteristics of the sampled images is displayed in Figure 7, which shows histograms of the four considered features for both the full dataset and the sampled subset. The histograms of individual features are not expected to be uniform since they represent a projection of the original data into one dimension. Still, it can be seen that the histograms of the sampled set tend to represent a slightly flattened version of the histograms of the original data, indicating that a larger priority is being given to atypical samples when compared to the original distribution. For instance, in the original data, the chances of selecting an image with a *typical* contrast (values in the range [0.18, 0.22]) are roughly 10 times larger than the chances of selecting an image with low contrast (lower than 0.12). On the other hand, the method defined a subset where the images with typical contrast are only around 5 times more frequent than low-contrast images.

A more robust way of visually checking the sampled subset is to visualize the data using Principal Component Analysis (PCA). Using PCA, the original 4-d data can be projected into 2-d with optimal preservation of the variance of the data. Figure 8 shows the PCA projection of the data. The four plots included in the figure represent the same projection, but the points are colored according to the different features used to characterize the images. It can be noticed that the sampling methodology selects a subset of images that uniformly covers the distribution of the data. Furthermore, as also suggested by the histograms in Figure 7, the sampling was capable

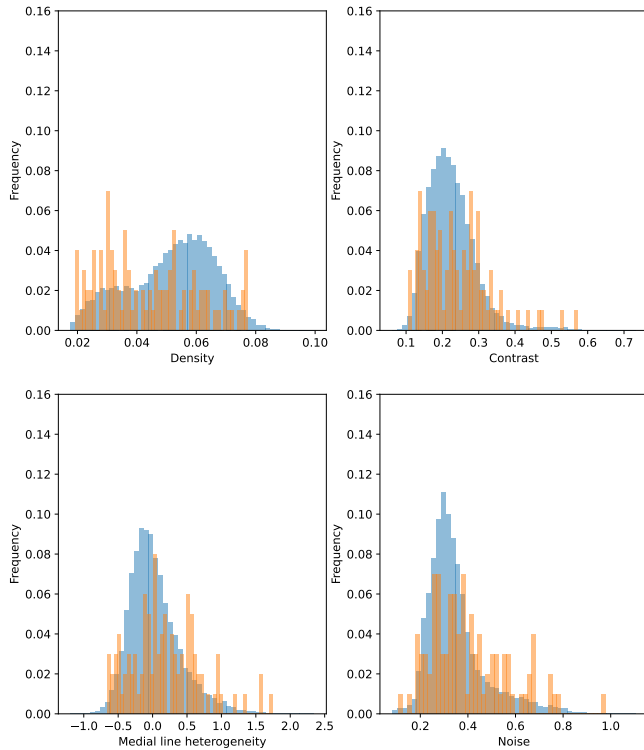


FIG. 7. Histograms of the four features that were calculated from the blood vessel dataset. Blue bars correspond to the distribution of the full data. Orange bars correspond to the distribution of the sampled subset. Note that the frequencies were normalized by their sum.

of covering the full range of values of every considered feature.

The subset of images selected by the method is shown in Figure 9. The subset indeed contains a heterogeneous set of images covering many different values of the considered features (e.g., low contrast, high vessel density, etc). This subset can then be manually annotated and used for training a machine learning algorithm to segment the full dataset. Since atypical samples are well-represented, we expect fewer biases in downstream analyses using the obtained segmentation. For instance, some of the samples in the dataset come from animals who suffered hemorrhagic strokes. These samples are very different from the typical samples contained in the dataset, and they would be largely underrepresented if a usual uniform sampling of the original data, which is associated with sampling the data according to its distribution, was performed.

IV. CONCLUSION

Selecting appropriate images for training machine learning algorithms is an important task that has been given relatively little attention. This is because the usual approach is to use as many images as possible. While this approach is relevant for general classification problems,

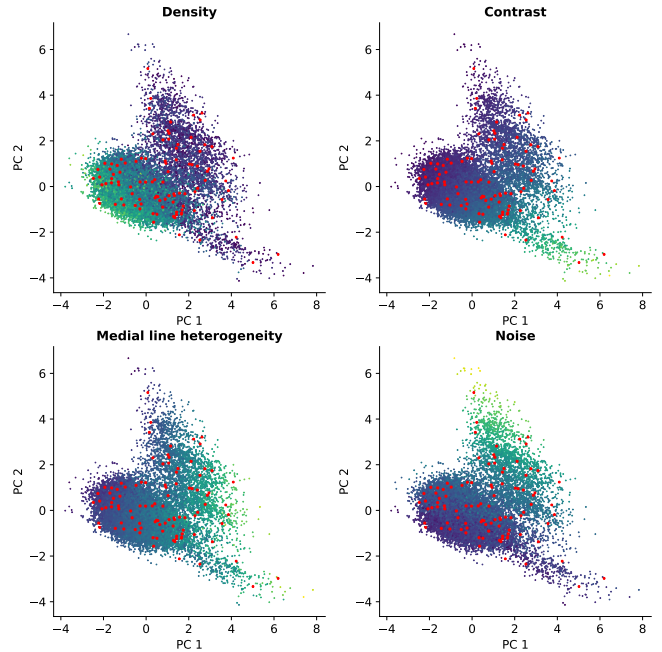


FIG. 8. PCA of the blood vessel dataset. For this projection, we used the original metric values with z-score normalization. Red points correspond to the sampled subset obtained by the sampling methodology. Other points correspond to the unselected points, with their colors representing the value of each one of the four original metrics: vessel density, contrast, medial line heterogeneity, and image noise.

for medical image segmentation, where image annotation can be very costly, the images used must be carefully selected in order to ensure good coverage of different tissue appearances and imaging variations. In addition, it is important that the selected images do not lead to biases in downstream tasks related to tissue characterization. For instance, we argued that training segmentation algorithms mostly on prototypical images can lead to incorrect measurements on samples having unusual properties (e.g., very bright or very noisy).

We developed an intuitive sampling methodology that evenly selects, as best as possible, both typical and atypical samples for creating a rich dataset that can then be annotated and used for training segmentation algorithms. One important property of the method is that it provides an intuitive uniform grid in the feature space that can be used for further analyses. For example, one can study the accuracy of the segmentation on different regions of the grid to identify regions where samples are not being correctly segmented. A robust algorithm should provide good segmentation no matter if a sample is too noisy, bright or dark, if it has low or high contrast or any other variation on relevant image properties. Likewise, expected tissue changes in the samples should not lead to variations in accuracy.

The method has only two parameters, the resolution and the radius of the hyperspherical structuring element.

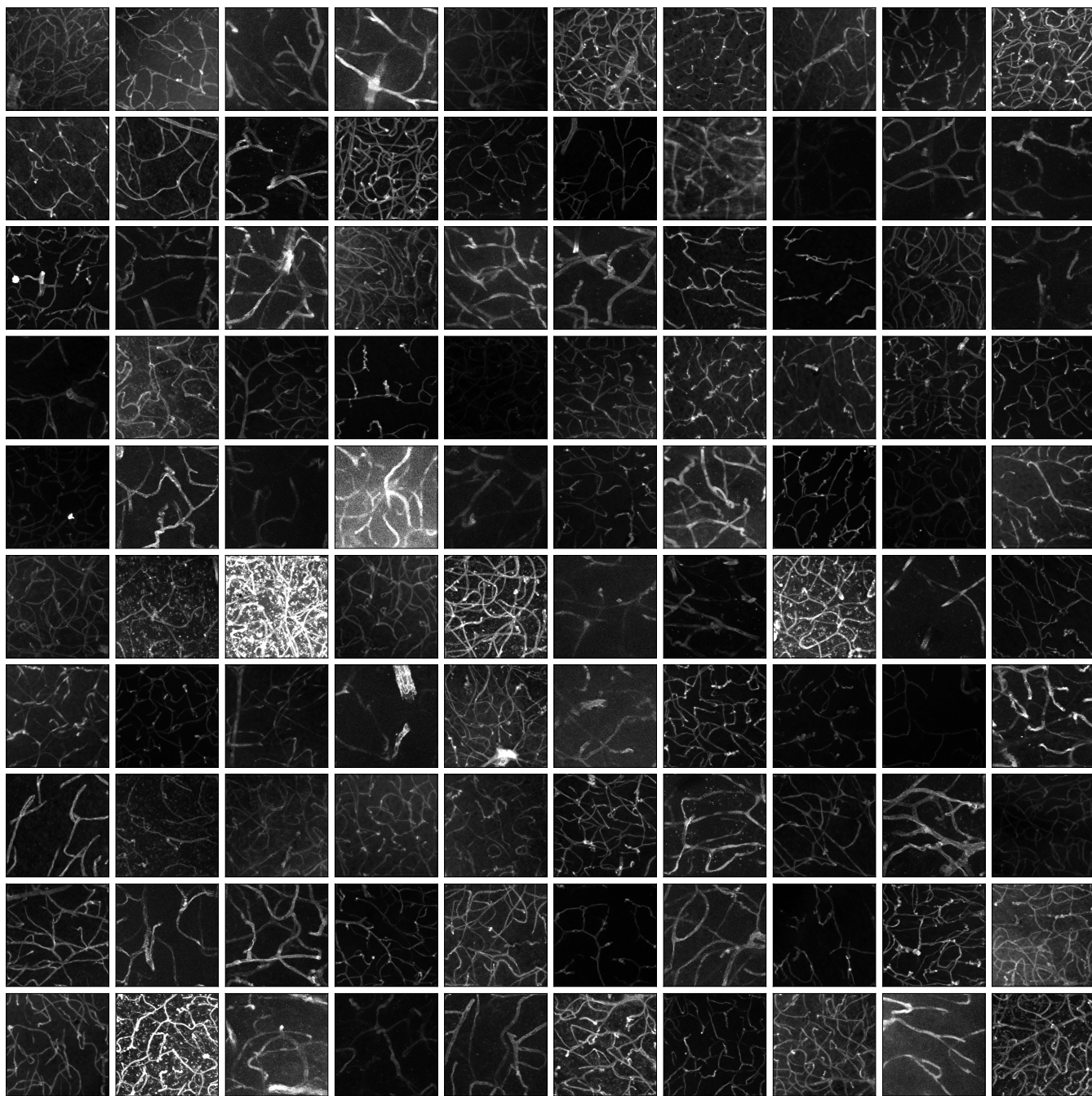


FIG. 9. Subset obtained by our methodology. Notice that the images cover a wide range of values in the feature space defined by our four features. Contrast variation and vessel density are the easier features to visually verify. Medial line heterogeneity can be verified by how much the brightness changes longitudinally within a blood vessel. Gaussian noise level is harder to verify visually, but pronounced noise can be observed on some of the brighter images.

The resolution can be set according to the scale in the feature space where images are expected to be very similar, and thus there is no need to consider multiple images with such a small variation in appearance. The radius of the hypersphere can be adjusted according to the average distance between points in the dataset. For instance, one can calculate the average distance between the near-

est neighbors of the dataset to gain intuition about the typical distances involved and then set the radius as a multiple of this distance.

We applied the methodology to a blood vessel dataset and showed that it can generate a heterogeneous set of samples representing many possible variations of image noise and contrast as well as blood vessel density and in-

tensity variance. A segmentation algorithm that can successfully identify the blood vessels on the selected images should generalize well on the whole dataset. More importantly, the selected samples guarantee that the algorithm will not focus only on the most prototypical samples, thus avoiding segmentation biases.

While the methodology was presented focusing on sample selection for annotation, it can also be used on any dataset to analyze possible performance biases. For instance, one could define an appropriate latent space for the ImageNet [35] and generate a subset of samples that uniformly covers the space. The performance of a robust

classifier should be similar in all regions of this space. Therefore, the sampling methodology presented here can also be used for interpreting so-called *black box* machine learning algorithms [36].

FUNDING

Cesar H. Comin thanks FAPESP (grant no. 21/12354-8) for financial support. The authors acknowledge the support of the Government of Canada’s New Frontiers in Research Fund (NFRF) (NFRFE-2019-00641) and Google’s Latin America Research Awards (LARA 2021).

-
- [1] Shutao Li, Weiwei Song, Leyuan Fang, Yushi Chen, Pedram Ghamisi, and Jón Atli Benediktsson, “Deep learning for hyperspectral image classification: An overview,” *IEEE Transactions on Geoscience and Remote Sensing* **57**, 6690–6709 (2019).
- [2] Lei Cai, Jingyang Gao, and Di Zhao, “A review of the application of deep learning in medical image classification and segmentation,” *Ann Transl Med* **8**, 713 (2020).
- [3] Syed Sahil Abbas Zaidi, Mohammad Samar Ansari, Asra Aslam, Nadia Kanwal, Mamoon Asghar, and Brian Lee, “A survey of modern deep learning based object detection models,” *Digital Signal Processing* **126**, 103514 (2022).
- [4] Shervin Minaee, Yuri Boykov, Fatih Porikli, Antonio Plaza, Nasser Kehtarnavaz, and Demetri Terzopoulos, “Image segmentation using deep learning: A survey,” *IEEE Transactions on Pattern Analysis and Machine Intelligence* **44**, 3523–3542 (2022).
- [5] Ian Goodfellow, Yoshua Bengio, and Aaron Courville, *Deep Learning* (MIT Press, 2016) <http://www.deeplearningbook.org>.
- [6] Olga Russakovsky, Jia Deng, Hao Su, Jonathan Krause, Sanjeev Satheesh, Sean Ma, Zhiheng Huang, Andrej Karpathy, Aditya Khosla, Michael Bernstein, Alexander C. Berg, and Li Fei-Fei, “ImageNet Large Scale Visual Recognition Challenge,” *International Journal of Computer Vision (IJCV)* **115**, 211–252 (2015).
- [7] Robert Geirhos, Kantharaju Narayanappa, Benjamin Mitzkus, Tizian Thieringer, Matthias Bethge, Felix A. Wichmann, and Wieland Brendel, “Partial success in closing the gap between human and machine vision,” in *Advances in Neural Information Processing Systems*, edited by A. Beygelzimer, Y. Dauphin, P. Liang, and J. Wortman Vaughan (2021).
- [8] Sarada M. W. Lee, Andrew Shaw, Jodie L. Simpson, David Uminsky, and Luke W. Garratt, “Differential cell counts using center-point networks achieves human-level accuracy and efficiency over segmentation,” *Scientific Reports* **11**, 16917 (2021).
- [9] Noah F. Greenwald, Geneva Miller, Erick Moen, Alex Kong, Adam Kagel, Thomas Dougherty, Christine Camacho Fullaway, Brianna J. McIntosh, Ke Xuan Leow, Morgan Sarah Schwartz, Cole Pavelchek, Sunny Cui, Isabella Camplisson, Omer Bar-Tal, Jaiveer Singh, Mara Fong, Gautam Chaudhry, Zion Abraham, Jackson Moseley, Shiri Warshawsky, Erin Soon, Shirley Greenbaum, Tyler Risom, Travis Hollmann, Sean C. Bendall, Leeat Keren, William Graf, Michael Angelo, and David Van Valen, “Whole-cell segmentation of tissue images with human-level performance using large-scale data annotation and deep learning,” *Nature Biotechnology* **40**, 555–565 (2022).
- [10] Qingquan Xu, Xiang Bai, and Wenyu Liu, “Multiple comparative attention network for offline handwritten chinese character recognition,” in *2019 International Conference on Document Analysis and Recognition (ICDAR)* (2019) pp. 595–600.
- [11] Suprosanna Shit, Johannes C. Paetzold, Anjany Sekuboyina, Andrey Zhylyka, Ivan Ezhov, Alexander Unger, Josien P. W. Pluim, Giles Tetteh, and Bjørn H. Menze, “cldice - a topology-preserving loss function for tubular structure segmentation.” *CoRR abs/2003.07311* (2020).
- [12] Agata Mosinska, Pablo Marquez-Neila, Mateusz Koziński, and Pascal Fua, “Beyond the pixel-wise loss for topology-aware delineation,” in *Proceedings of the IEEE conference on computer vision and pattern recognition* (2018) pp. 3136–3145.
- [13] Matheus V. da Silva, Julie Ouellette, Baptiste Lacoste, and Cesar H. Comin, “An analysis of the influence of transfer learning when measuring the tortuosity of blood vessels,” *Computer Methods and Programs in Biomedicine* **225**, 107021 (2022).
- [14] Ahmad Chaddad, Jihao Peng, Jian Xu, and Ahmed Bouridane, “Survey of explainable ai techniques in healthcare,” *Sensors* **23** (2023), 10.3390/s23020634.
- [15] Rodrigo de P. Mendes, Xin Yuan, Elizabeth M. Genega, Xiaoyin Xu, Luciano da F. Costa, and Cesar H. Comin, “Gland context networks: A novel approach for improving prostate cancer identification,” *Computerized Medical Imaging and Graphics* **94**, 101999 (2021).
- [16] Julián Pérez-Beteta, David Molina-García, José A. Ortiz-Alhambra, Antonio Fernández-Romero, Belén Luque, Elena Arregui, Manuel Calvo, José M. Borrás, Bárbara Meléndez, Ángel Rodríguez de Lope, Raquel Moreno de la Presa, Lidia Iglesias Bayo, Juan A. Barcia, Juan Martino, Carlos Velásquez, Beatriz Asenjo, Manuel Benavides, Ismael Herruzo, Antonio Revert, Estanislao Arana, and Víctor M. Pérez-García, “Tumor surface regularity at mr imaging predicts survival and response to surgery in patients with glioblas-

- toma,” *Radiology* **288**, 218–225 (2018), pMID: 29924716, <https://doi.org/10.1148/radiol.2018171051>.
- [17] Johannes C. Paetzold, Julian McGinnis, Suprosanna Shit, Ivan Ezhov, Paul Büschl, Chinmay Prabhakar, Anjany Sekuboyina, Mihail Todorov, Georgios Kaissis, Ali Ertürk, Stephan Günemann, and bjoern menze, “Whole brain vessel graphs: A dataset and benchmark for graph learning and neuroscience,” in *Thirty-fifth Conference on Neural Information Processing Systems Datasets and Benchmarks Track (Round 2)* (2021).
- [18] Moises Freitas-Andrade, Cesar H. Comin, Matheus Viana da Silva, Luciano F. Fontoura Da Costa, and Baptiste Lacoste, “Unbiased analysis of mouse brain endothelial networks from two- or three-dimensional fluorescence images,” *Neurophotonics* **9**, 031916 (2022).
- [19] Alice Krestanova, Jan Kubicek, and Marek Penhaker, “Recent techniques and trends for retinal blood vessel extraction and tortuosity evaluation: A comprehensive review,” *Ieee Access* **8**, 197787–197816 (2020).
- [20] Annika Reinke, Minu D. Tizabi, Carole H. Sudre, Matthias Eisenmann, Tim Rädtsch, Michael Baumgartner, Laura Acion, Michela Antonelli, Tal Arbel, Spyridon Bakas, Peter Bankhead, Arriel Benis, M. Jorge Cardoso, Veronika Cheplygina, Evangelia Christodoulou, Beth Cimini, Gary S. Collins, Keyvan Farahani, Bram van Ginneken, Ben Glocker, Patrick Godau, Fred Hamprecht, Daniel A. Hashimoto, Doreen Heckmann-Nötzel, Michael M. Hoffman, Merel Huisman, Fabian Isensee, Pierre Jannin, Charles E. Kahn, Alexandros Karargyris, Alan Karthikesalingam, Bernhard Kainz, Emre Kavur, Hannes Kennigott, Jens Kleesiek, Thijs Kooi, Michal Kozubek, Anna Kreshuk, Tahsin Kurc, Bennett A. Landman, Geert Litjens, Amin Madani, Klaus Maier-Hein, Anne L. Martel, Peter Mattson, Erik Meijering, Bjoern Menze, David Moher, Karel G. M. Moons, Henning Müller, Brennan Nichyporuk, Felix Nickel, M. Alican Noyan, Jens Petersen, Gorkem Polat, Nasir Rajpoot, Mauricio Reyes, Nicola Rieke, Michael Riegler, Hassan Rivaz, Julio Saez-Rodriguez, Clarisa Sanchez Gutierrez, Julien Schroeter, Anindo Saha, Shravya Shetty, Maarten van Smeden, Bram Stieltjes, Ronald M. Summers, Abdel A. Taha, Sotirios A. Tsaftaris, Ben Van Calster, Gaël Varoquaux, Manuel Wiesenfarth, Ziv R. Yaniv, Annette Kopp-Schneider, Paul Jäger, and Lena Maier-Hein, “Common limitations of image processing metrics: A picture story,” (2021).
- [21] Rémi Domingues, Maurizio Filippone, Pietro Michiardi, and Jihane Zouaoui, “A comparative evaluation of outlier detection algorithms: Experiments and analyses,” *Pattern Recognition* **74**, 406–421 (2018).
- [22] Hongzhi Wang, Mohamed Jaward Bah, and Mohamed Hammad, “Progress in outlier detection techniques: A survey,” *IEEE Access* **7**, 107964–108000 (2019).
- [23] Chengcheng Guo, Bo Zhao, and Yanbing Bai, “Deepcore: A comprehensive library for coresets selection in deep learning,” in *Database and Expert Systems Applications*, edited by Christine Strauss, Alfredo Cuzzocrea, Gabriele Kotsis, A. Min Tjoa, and Ismail Khalil (Springer International Publishing, Cham, 2022) pp. 181–195.
- [24] Hao Zheng, Lin Yang, Jianxu Chen, Jun Han, Yizhe Zhang, Peixian Liang, Zhuo Zhao, Chaoli Wang, and Danny Z Chen, “Biomedical image segmentation via representative annotation,” in *Proceedings of the AAAI Conference on Artificial Intelligence*, Vol. 33 (2019) pp. 5901–5908.
- [25] Bishwo Adhikari, Esa Rahtu, and Heikki Huttunen, “Sample selection for efficient image annotation,” in *2021 9th European Workshop on Visual Information Processing (EUVIP)* (2021) pp. 1–6.
- [26] Lin Yang, Yizhe Zhang, Jianxu Chen, Siyuan Zhang, and Danny Z. Chen, “Suggestive annotation: A deep active learning framework for biomedical image segmentation,” in *Medical Image Computing and Computer Assisted Intervention - MICCAI 2017*, edited by Maxime Descoteaux, Lena Maier-Hein, Alfred Franz, Pierre Jannin, D. Louis Collins, and Simon Duchesne (Springer International Publishing, Cham, 2017) pp. 399–407.
- [27] Asim Smailagic, Pedro Costa, Hae Young Noh, Divesh Walawalkar, Kartik Khandelwal, Adrian Galdran, Mostafa Mirshekari, Jonathon Fagert, Susu Xu, Pei Zhang, and Aurélio Campilho, “Medal: Accurate and robust deep active learning for medical image analysis,” in *2018 17th IEEE International Conference on Machine Learning and Applications (ICMLA)* (2018) pp. 481–488.
- [28] Firat Ozdemir, Zixuan Peng, Christine Tanner, Philipp Fuernstahl, and Orcun Goksel, “Active learning for segmentation by optimizing content information for maximal entropy,” in *Deep Learning in Medical Image Analysis and Multimodal Learning for Clinical Decision Support*, edited by Danail Stoyanov, Zeike Taylor, Gustavo Carneiro, Tanveer Syeda-Mahmood, Anne Martel, Lena Maier-Hein, João Manuel R.S. Tavares, Andrew Bradley, João Paulo Papa, Vasileios Belagiannis, Jacinto C. Nascimento, Zhi Lu, Sailesh Conjeti, Mehdi Moradi, Hayit Greenspan, and Anant Madabhushi (Springer International Publishing, Cham, 2018) pp. 183–191.
- [29] Ozan Sener and Silvio Savarese, “Active learning for convolutional neural networks: A core-set approach,” in *International Conference on Learning Representations* (2018).
- [30] Baptiste Lacoste, Cesar H. Comin, Ayal Ben-Zvi, Pascal S. Kaeser, Xiaoyin Xu, Luciano da F. Costa, and Chenghua Gu, “Sensory-related neural activity regulates the structure of vascular networks in the cerebral cortex,” *Neuron* **83**, 1117–1130 (2014).
- [31] Ayden Gouveia, Matthew Seegobin, Timal S. Kannagara, Ling He, Fredric Wondisford, Cesar H. Comin, Luciano da F. Costa, Jean-Claude Béique, Diane C. Lagace, Baptiste Lacoste, and Jing Wang, “The apk-cbp pathway regulates post-stroke neurovascular remodeling and functional recovery,” *Stem Cell Reports* **9**, 1735–1744 (2017).
- [32] Julie Ouellette, Xavier Toussay, Cesar H. Comin, Luciano da F. Costa, Mirabelle Ho, María Lacalle-Aurioles, Moises Freitas-Andrade, Qing Yan Liu, Sonia Leclerc, Youlian Pan, Ziyang Liu, Jean-François Thibodeau, Melissa Yin, Micael Carrier, Cameron J. Morse, Peter Van Dyken, Christopher J. Bergin, Sylvain Baillet, Christopher R. Kennedy, Marie-Ève Tremblay, Yannick D. Benoit, William L. Stanford, Dylan Burger, Duncan J. Stewart, and Baptiste Lacoste, “Vascular contributions to 16p11.2 deletion autism syndrome modeled in mice,” *Nature Neuroscience* **23**, 1090–1101 (2020).
- [33] David L Donoho and Iain M Johnstone, “Ideal spatial adaptation by wavelet shrinkage,” *Biometrika* **81**, 425–455 (1994), <https://academic.oup.com/biomet/article-pdf/81/3/425/26079146/81.3.425.pdf>.

- [34] Kàlmàn Palàgyi and Attila Kuba, “A 3d 6-subiteration thinning algorithm for extracting medial lines,” *Pattern Recognition Letters* **19**, 613–627 (1998).
- [35] J. Deng, W. Dong, R. Socher, L.-J. Li, K. Li, and L. Fei-Fei, “ImageNet: A Large-Scale Hierarchical Image Database,” in *CVPR09* (2009).
- [36] Cynthia Rudin, “Stop explaining black box machine learning models for high stakes decisions and use interpretable models instead,” *Nature Machine Intelligence* **1**, 206–215 (2019).